

Fatigue Crack Growth Behavior of a Solid Solution-Strengthened Nickel-Base Superalloy (Incoloy 825)

L. Bartosiewicz, A.R. Krause, A. Spis, J. Raghavan, and S.K. Putatunda

Fatigue crack growth behavior of a solid solution-strengthened nickel-base superalloy (Incoloy 825)* was investigated. The investigation also examined the influence of heat treatment on resultant microstructures and the near-threshold fatigue crack growth behavior. In addition, the influence of load ratios (R), material strength, and grain size on fatigue threshold was studied. Compact tension specimens prepared from Incoloy 825 with transverse-longitudinal (TL) orientation in the as-received, as well as two different heat treated conditions, were used. The heat treatment studies revealed a peak hardness condition after solution treatment at 1200 °C for 1/2 hr, followed by aging at 600 °C for 434 hr. Among all the heat treated conditions, the fatigue threshold was the highest and the near-threshold crack growth rate was lowest in this peak aged condition. Fatigue threshold values were observed to decrease with an increase in load ratio, whereas an increased grain diameter resulted in a higher fatigue threshold. An earlier mathematical model was found applicable to characterize the relationship between load ratio and fatigue threshold. Preferential etching of grain boundary suggests formation of a thin film of carbide precipitation along the grain boundary region in the aged specimens. This carbide precipitation facilitated intergranular crack growth in these samples, resulting in higher roughness-induced crack closure. The highest fatigue threshold in the peak aged condition can be attributed to this large roughness-induced crack closure process.

1 Introduction

FATIGUE crack growth rate (da/dN) has been related to the stress-intensity range (ΔK), and the Paris equation[1] has been found to be useful to characterize fatigue crack growth behavior. The Paris equation relates the crack growth rate with the stress-intensity range in the form of a power law equation:

$$da/dN = C(\Delta K)^m$$

where C and m are material constants and $\Delta K = K_{max} - K_{min}$ is the difference between maximum and minimum stress-intensity factors.

However, when the experimental crack growth rate data are plotted against the stress-intensity range in a log-log scale, a sigmoidal curve (Fig. 1) with varying slopes is obtained, as opposed to a linear plot as predicted by the Paris equation. There are three distinct regions in this plot. In Region I, or the threshold region, the crack growth rate is slow and deviates from the Paris equation. In the linear region (Region II), the Paris equation is usually obeyed by most materials, and the crack growth rate increases linearly with the stress-intensity factor. In Region III, or the fast fracture region, the crack growth rate accelerates and again deviates from the Paris equation. In addition to all three regions, there is also a threshold stress-intensity factor (ΔK_{th}), below which the crack growth rate approaches a zero value.

The threshold region[2] is very important, because a significant portion of life of a structural component is spent in this region. Threshold stress-intensity factor is also a very important parameter for structural design because structural components designed on the basis of fatigue threshold are expected to have infinite lives.

Numerous variables[3-11] can affect the near-threshold fatigue crack growth rate and the fatigue threshold. However, from a practical point of view, the influences of microstructure and the load ratio are most important. Earlier workers[3-11] have shown that in a wide range of materials by modification of the microstructure it may be possible to increase the fatigue threshold and decrease the near-threshold crack growth rate. However, most of these investigations were carried out in alloy steels, titanium, aluminum alloys, etc. and limited information is available about the influence of microstructure on fatigue threshold, or on the near-threshold crack growth behavior of nickel-base superalloys, particularly solid solution-strengthened nickel-base superalloys.

Incoloy 825 is a solid solution-strengthened nickel-base superalloy. This material is used extensively in many high-temperature applications such as piping material in steam boilers,

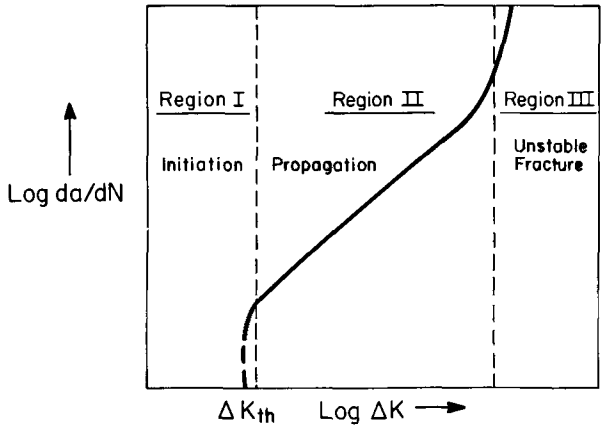

Fig. 1 Schematic representation of fatigue crack growth according to Paris equation.

L. Bartosiewicz, Staff Scientist, Research Staff, Ford Motor Company; **A.R. Krause,** Research Scientist Senior, Research Staff, Ford Motor Company; Dearborn, Michigan; **A. Spis** and **J. Raghavan,** Graduate Students, Department of Materials Science and Engineering, Wayne State University; and **S.K. Putatunda,** Associate Professor, Department of Materials Science and Engineering, Wayne State University, Detroit, Michigan.

*Incoloy 825 is a trademark for products of Huntington Alloys, Inc.

lining material in bag house scrubbers, high-temperature pressure vessels, etc. The present investigation examines the influence of microstructure on near-threshold fatigue crack growth rate and fatigue threshold at room temperature and ambient atmosphere for this material.

2 Experimental Procedures

2.1 *Material*

The material used in this study was Incoloy 825. It was available in the form of a cold rolled 1/2-in. thick plate with identifiable rolling direction from Huntington Alloys, Inc. The chemical composition of the material is reported in Table 1.

2.2 *Specimen Preparation*

Compact tension specimens with transverse-longitudinal (TL) orientation were prepared as per ASTM E-647.[12] A schematic of the specimens used in this study is shown in Fig. 2. The initial aspect ratio was kept at (crack length to width) $a/W = 0.40$.

Table 1 Chemical Composition of Test Material

Element	Composition, wt%
Cr	20.2
Al	0.2
Ti	1.10
Mo	2.8
Cu	2.1
Fe	23.5
Mn	0.85
S	0.02
C	0.046
Ni	Bal

Table 2 Heat Treatment Procedures

Specimen	Heat treatment	Average grain diameter, μm
A	As received	70
B	Solution treated at 1200 °C for 1/2 hr and aged at 600 °C for 118 hr	138
C	Solution treated at 1200 °C for 1/2 hr and aged at 600 °C for 434 hr	140

After fabrication, the specimens were subjected to two different heat treatments. These heat treatment conditions are identified as B and C, whereas the as-received material (without heat treatment) will be identified as A. All subsequent references to the specimens in text are based on these letter designations. Details of the heat treatment procedures and the resulting average grain diameters are reported in Table 2. The mechanical properties of the materials before and after heat treatments are listed in Table 3.

2.3 *Fatigue Testing*

After heat treatment, the specimens were ground on both surfaces and subsequently polished with 600-grit emery paper. This was found to be very helpful in locating the crack tip during fatigue testing. All the specimens were initially precracked in fatigue at a ΔK level of $\Delta K = 15$ MPa$\sqrt{m}$ to produce a 2-mm long sharp crack front. After precracking, the fatigue testing was carried out using an MTS servohydraulic test machine in the load control mode. All tests were carried out at room temperature in ambient atmosphere using tension-tension mode. A constant-amplitude sinusoidal wave form was applied, and the fatigue testing was carried out at several load ratios (R) such as $R = 0.10$, 0.50, and 0.90, respectively. The crack lengths were monitored continuously with the help of an optical traveling microscope, and the crack growth rates were determined according to ASTM E-647.[12] The fatigue threshold was determined using the load shedding technique of ASTM E-647[12] and the threshold was identified graphically by plotting log da/dN versus log ΔK. The

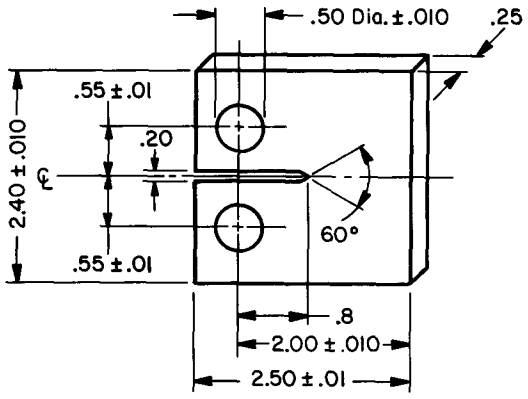

Fig. 2 Compact tension specimen (2T). Scale: full size; all dimensions in inches.

Table 3 Mechanical Properties of Test Specimens

Sample	Condition	Yield strength (0.2%), MPa	Ultimate tensile strength, MPa	Reduction in area, %	Strain-hardening exponent, *n*	Total elongation, %
A	As received	337	686	47	0.14	30
B	Solution treated for 1/2 hr at 1200 °C and aged at 600 °C for 118 hr	250	632	57	0.18	55
C	Solution treated for 1/2 hr at 1200 °C and aged at 600 °C for 434 hr	315	745	48	0.16	55

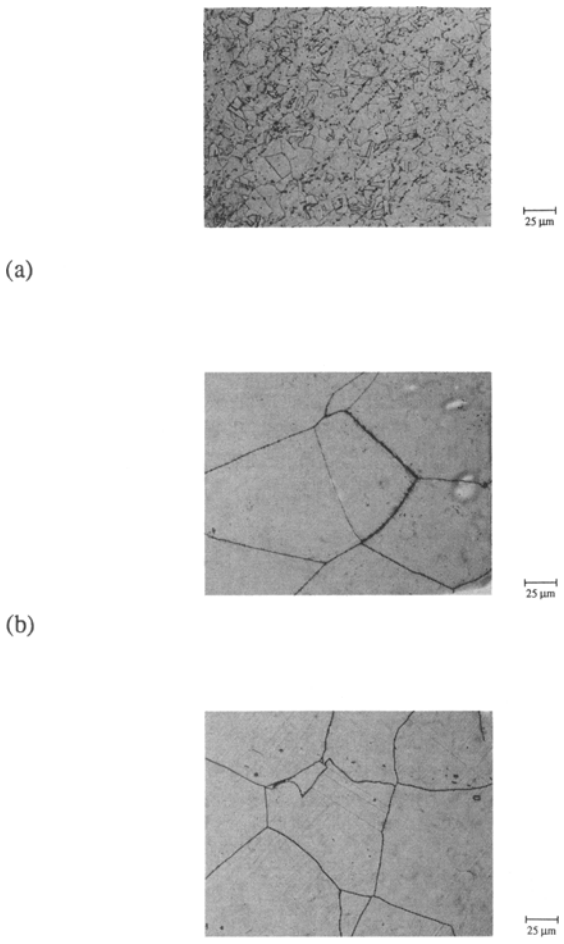

Fig. 3(a) As-received cold rolled alloy plate. 400× magnification. **(b)** Aged at 600 °C for 118 hr. 400× magnification. **(c)** Aged at 600 °C for 434 hr (peak aged). 400× magnification.

threshold was identified as the value of ΔK at which the crack growth rate was of the order of 10^{-10} m/cycle.

3 Results and Discussions

3.1 *Heat Treatments and Microstructure*

The microstructure of the as-received material (A) is shown in Fig. 3(a), and the microstructures of the heat treated samples B and C are shown in Fig. 3(b) and 3(c). The mechanical properties of the materials are reported in Table 3. A thorough heat treatment study was initially conducted where the specimens were solution treated and then aged at 600 °C for various periods. This is reported in Fig. 4. Heat treatment studies indicated a peak hardness condition with very high yield strength after solution treatment at 1200 °C for 1/2 hr and aging at 600 °C for 434 hr. Moreover, this heat treat condition (Sample C) produced an approximate twofold increase in grain diameter (Table 2).

Generally, all microstructures had an austenitic matrix with a considerable amount of twins present. After solution treatment

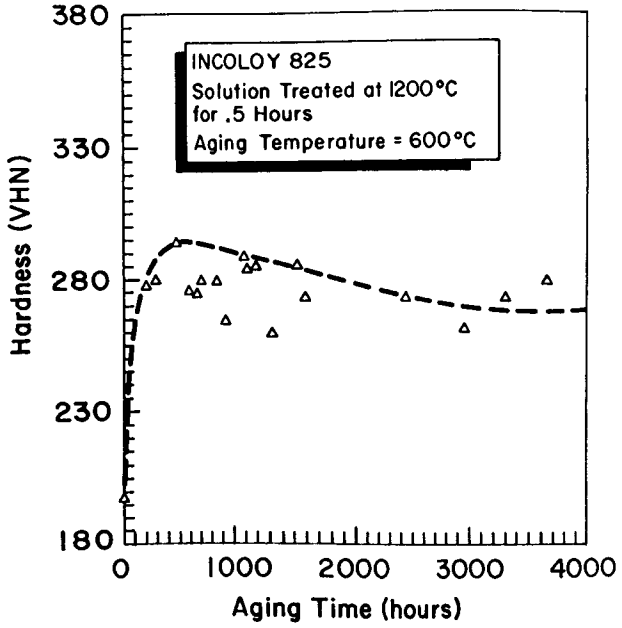

Fig. 4 Hardness versus aging time.

and aging, a gradual precipitation of carbides was observed with transmission electron microscopy (TEM). The TEM microanalytical studies[13] revealed several specifics:

- The matrix is mainly Fe, Cr, and Ni.
- After solution treatment and aging at 600 °C, $M_{23}C_6$-type precipitation occurred in heat treated conditions B and C.
- In heat treated conditions of Samples B and C, spherical precipitates of approximately 0.18-μm diameter were observed. These were identified as Ti and Cr carbides. In addition to these, there were very fine precipitates in Sample C, which could not be identified by EDAX because of their extreme fineness. These precipitates appear to be γ'.
- Preferential etching of grain boundaries in Sample C suggests the presence of a continuous carbide film with an average width of 2 to 3 μm. Transmission electron microscopy further[13] verified that these carbides reside at grain boundaries in a continuous morphology. Some earlier workers[14] have also reported similar phenomenon occurring in nickel-base superalloys after aging at relatively low temperatures.
- Hardness and aging time relations are represented in Fig. 4, showing a peak hardness of 295 VHN after aging at 600 °C for 434 hr. The hardness of the specimens starts decreasing after aging beyond this period.

It has been reported[15] that in those solid solution-strengthened nickel-base superalloys where the combined amount of aluminum and titanium is less than 2 wt%, γ' precipitates do not occur. However, in spite of the lesser amount of these elements (Al and Ti), our investigations indicate that the γ' precipitate is probably taking place in Sample C. However, as mentioned earlier, because of the extreme fineness of these particles, it could not be determined with certainty that they are indeed γ'. The formation of spherical Ti and Cr carbides increased both the hardness and strength of Samples B and C. The significance of car-

bide film formation along the grain boundaries will be discussed later.

3.2 *Influence of Microstructure on Fatigue Crack Growth Rate*

Figure 5 compares the fatigue crack growth ratio of materials in heat treated conditions A, B, and C. The load ratio ($R = 0.10$) was identical for these specimens. The Paris constants C and m for these specimens are reported in Table 4. In Fig. 6, the fatigue crack growth rate of Specimens A, B, and C are compared at the same load ratio of $R = 0.50$. Table 5 reports the fatigue threshold values of the materials in different heat treated conditions.

The results shown in Fig. 5 and 6 indicate that in the threshold region the crack growth rate for Sample C is approximately a magnitude lower than that of Sample A. As mentioned earlier, Sample C had the highest hardness and yield strength among the heat treated samples. The lower crack growth rate in the threshold region of this sample (C) has resulted in a significant increase in fatigue threshold, as reported in Table 5. Moreover, Fig. 5 and 6 show the trend that as ΔK increases the differences in crack growth rates between the non-heat treated sample (A) and the heat treated samples (B and C) gradually decreases. Furthermore, comparing the test results of Fig. 5 and 6, we observe that the near threshold crack growth rate increases with the increase in load ratio.

As mentioned earlier, test results in Fig. 5 and 6 show that Sample C has the lowest near-threshold crack growth rate and highest fatigue threshold than other samples. Incidentally, in most materials, fatigue threshold decreases with the increase in yield strength. In addition, the near-threshold crack growth rate in most materials increases with an increase in hardness. Hence,

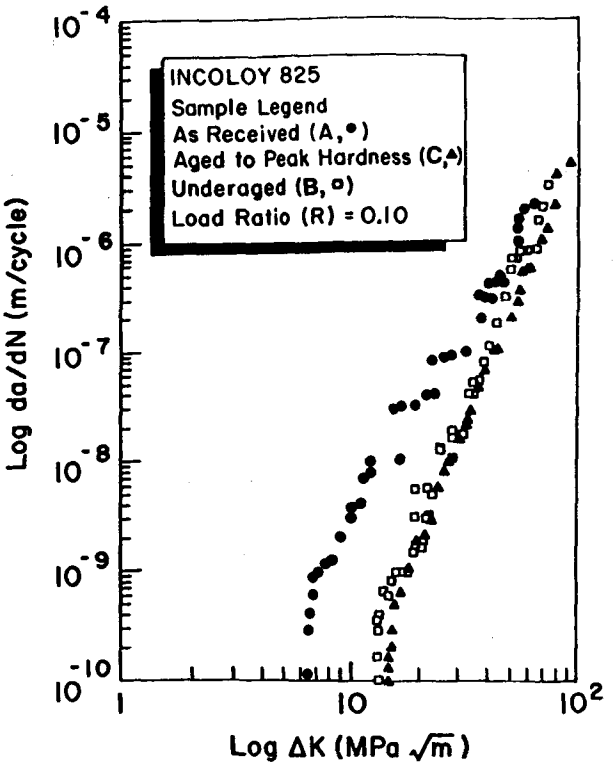

Fig. 5 Effect of heat treatment on fatigue crack growth rate.

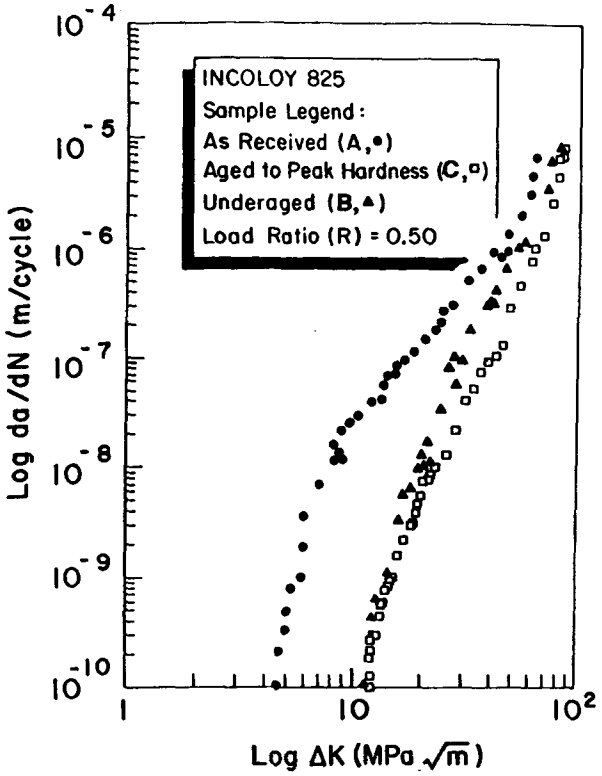

Fig. 6 Effect of heat treatment on fatigue crack growth rate.

Table 4 Paris Constants of Test Specimens

Sample	Condition	Load ratio	Paris Constants m	Paris Constants C
A	Non-heat treated	0.1	3.5	1×10^{-12}
		0.5	3.0	$1\times10^{-10.8}$
		0.9	2.9	$1\times10^{-10.7}$
B	Under aged	0.1	4.9	1×10^{-15}
		0.5	4.7	1×10^{-13}
C	Aged to peak hardness	0.1	5.0	$1\times10^{-15.1}$
		0.5	4.8	$1\times10^{-14.3}$

a higher near-threshold crack growth rate and a lower fatigue threshold was expected in Sample C. However, our results (Fig. 5 and 6 and Table 5) indicate that, with a suitable heat treatment process, it is possible to simultaneously increase yield strength and fatigue threshold of the material.

The higher fatigue threshold and lower crack growth rate in the threshold region for Samples B and C can be explained on the basis of the crack closure[15] phenomenon. During cyclic loading, a cyclic plastic zone is induced at the crack tip and the residual compressive stresses in the cyclic plastic zone causes a partial closure of the crack tip. Due to this crack closure, the effective stress-intensity factor ($\Delta K_{eff} = K_{max} - K$op) decreases or, in other words, the mechanical driving force for crack propagation decreases. Besides this cyclic plasticity-induced crack closure, crack closure can also be produced by several other mechanisms such as corrosion by-products, fracture surface roughness, oxides, etc.[16-18] In Sample C, the crack path was mostly intergranular and followed an irregular trajectory. Figure 7 shows a schematic of the crack path in Sample C. On the other hand, in Sample A, the crack path was mostly straight and mostly transgranular[13] in nature. Again, the grain size of Sample A was approximately half of that of Sample C. During the aging process, a thin carbide film forms in the grain boundary region of Sample C. This film is extremely brittle[19] and fractures during the cyclic loading. The ensuing process facilitates the crack propagation along the grain boundaries and produces an irregular trajectory. The net result in Sample C is a larger amount of surface roughness-induced crack closure, resulting in a very high fatigue threshold.

This crack trajectory along the grain boundaries in Sample C causes a significant increase in roughness-induced crack closure due to the very large grain size (148 μm) and substantially reduces the effective stress-intensity factor. This has resulted in a high fatigue threshold and a lower near-threshold crack growth rate. Figure 8 shows the fracture surface of Samples A and C. Be-

Table 5 Fatigue Threshold at Load Ratio $R = 0.1$

Sample	Material condition	ΔK_{th}, MPA$\sqrt{m}$
A	As received	6.6
B	Solution treated for 1/2 hr at 1200 °C and aged at 600 °C for 118 hr	12.2
C	Solution treated for 1/2 hr at 1200 °C and aged at 600 °C for 434 hr	14.4

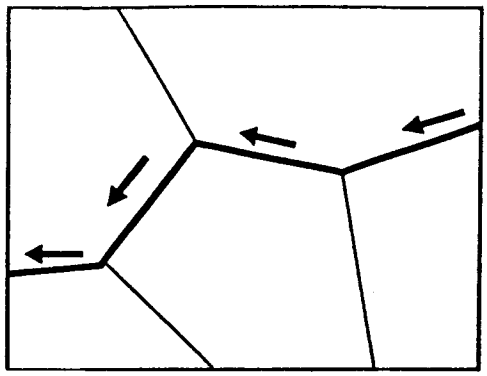

(a)

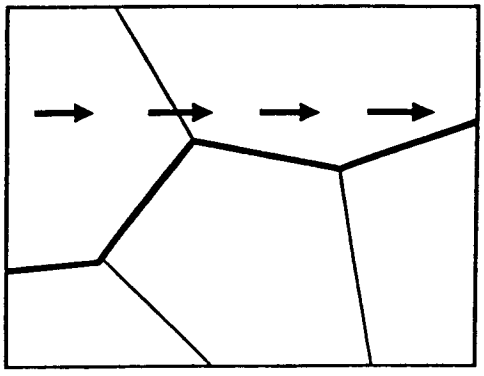

(b)

Fig. 7(a) Schematic diagram of intergranular crack path in Incoloy 825. Samples B and C. **(b)** Schematic diagram of transgranular crack path in Sample A.

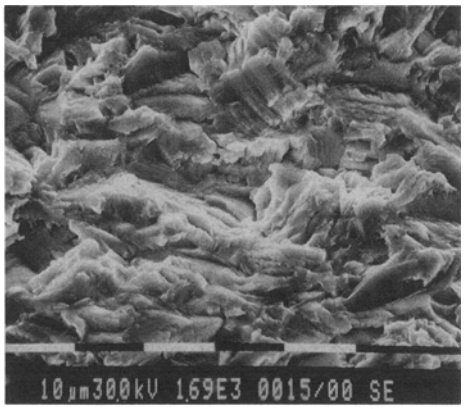

(a)

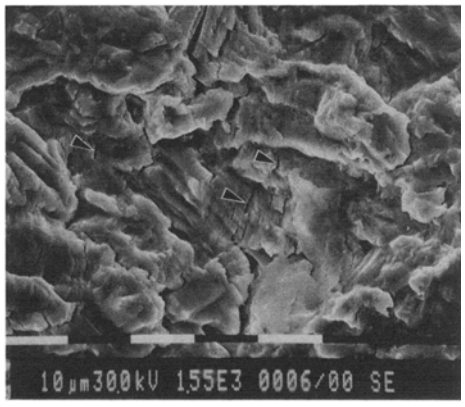

(b)

Fig. 8(a) Sample A, minimal crack branching. **(b)** Sample C, extensive crack branching in Incoloy 825.

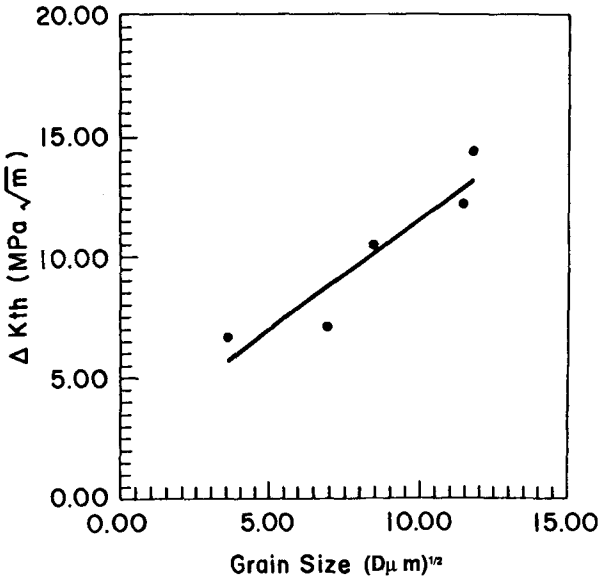

Fig. 9 Effect of grain size on fatigue threshold in Incoloy 825.

sides this irregular crack trajectory, in Sample C extensive secondary crackings were observed (some marked with arrows in Fig. 8), and in Sample A, the similar crack branching was not generally seen. This crack branching also decreases the crack driving energy and hence results in a significantly higher fatigue threshold in Sample C.

3.3 *Influence of Grain Size and Yield Strength on Fatigue Threshold*

In this study, one of the main reasons for examining the effect of different heat treatments on fatigue threshold was to elucidate the individual effect of grain size and yield strength on fatigue threshold. This is accomplished by comparing the fatigue thresholds of Samples B and C. These samples have similar grain sizes (Table 2), but different yield strengths (Table 3). These results clearly show that higher yield strength can increase the fatigue threshold.

Figure 9 is a plot of the fatigue threshold and grain size for the samples, including the result of different heat treatments (A, B, and C). The plot shows that fatigue threshold tends to increase with an increase in grain diameter.

3.4 *Influence of Load Ratio on Fatigue Crack Growth Rate and Fatigue Threshold*

Figures 10, 11, and 12 report the influence of load ratio on the fatigue crack growth rate in the threshold region for Samples A, B, and C. It is evident that, as the load ratio (R) increases, the fatigue crack growth rate in the threshold region increases in these samples. However, it is apparent that the difference in increase in the crack growth rate, with the increase in load ratios, is higher for Sample A. Furthermore, comparing the results in Fig. 10, 11, and 12, we observe that the effect of the load ratios on crack growth is much smaller in the linear region than in the threshold region.

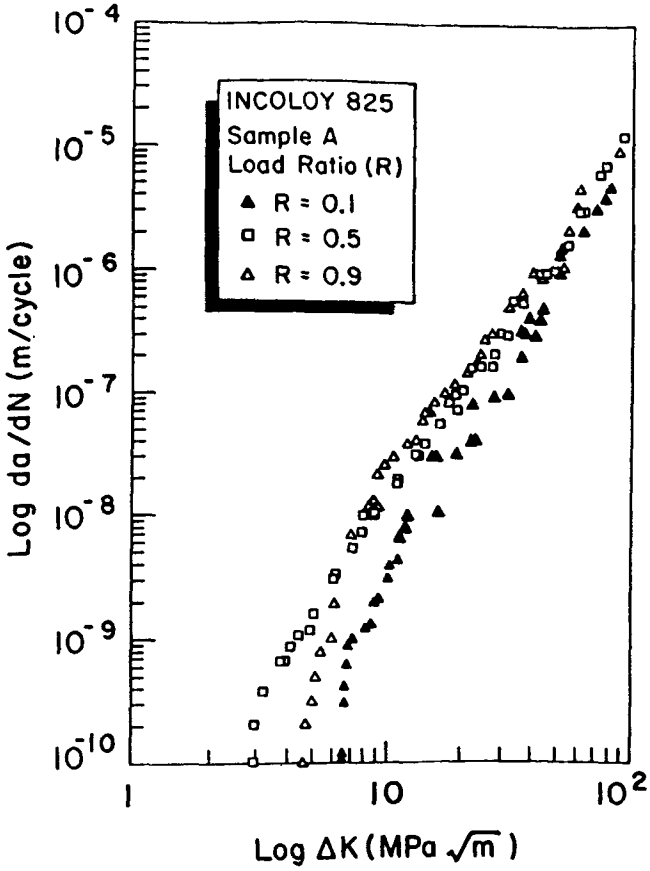

Fig. 10 Effect of load ratio on fatigue crack growth rate.

In Fig. 13, the fatigue threshold is plotted against load ratio R. It is apparent that the threshold decreases with an increase in the load ratio. This is because, at higher R values (R = 0.50 and 0.90), the crack is *always open*. Hence, the effect of crack closure is greatly diminished at high load ratios. However, it is reasonable to expect that under this condition the fatigue threshold in both samples (A and C) would be more or less equal. However, we observe that even at high load ratios R = 0.5 and 0.9, the threshold values for Samples B and C are very high. The reason for this is that even at high load ratios, a significant amount of surface roughness-induced crack closures can occur in Samples B and C. Many earlier works have also shown[19] that significantly large amounts of roughness-induced crack closure can take place even at high load ratios in certain situations. However, the fatigue threshold values of Samples B and C are relatively equal at high load ratios (Table 6). This is due to the similar nature of crack propagation (intergranular) in Samples B and C, which produces significant amounts of crack closure in both these specimens even at high load ratios.

Vosikovsky[20] analyzed the data from the literature concerning the effect of load ratio on fatigue threshold. He reported that in most cases the threshold values decrease with an increase in the load ratio. He also proposed an empirical relationship, of the nature $\Delta K_{th} = \Delta K_{tho}(1 - bR)$, where ΔK_{tho} is the value of threshold at load ratio R = 0, and b is a material-specific constant. Furthermore, he observed that both ΔK_{tho} and b tend to decrease

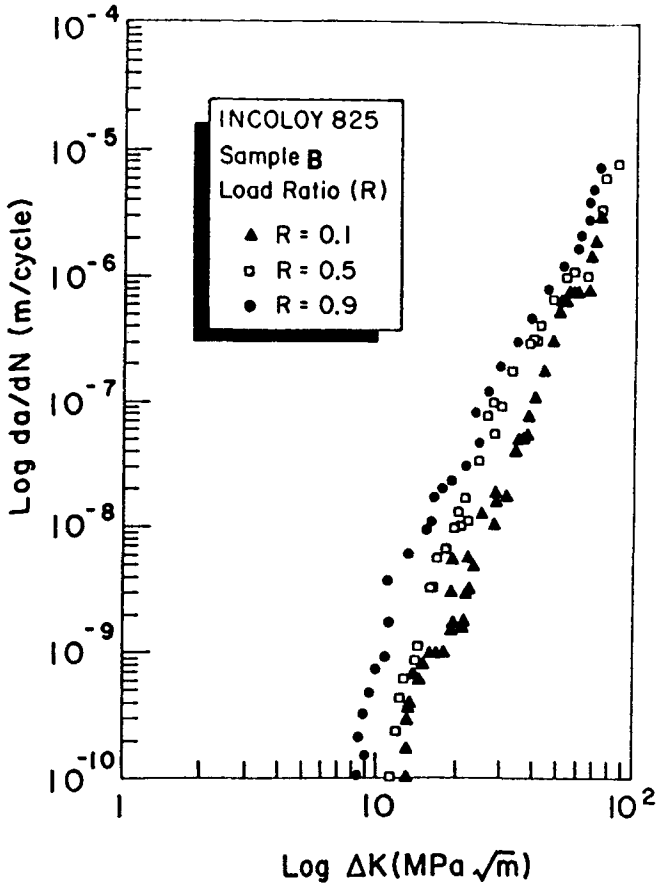

Fig. 11 Effect of ratio on fatigue crack growth rate.

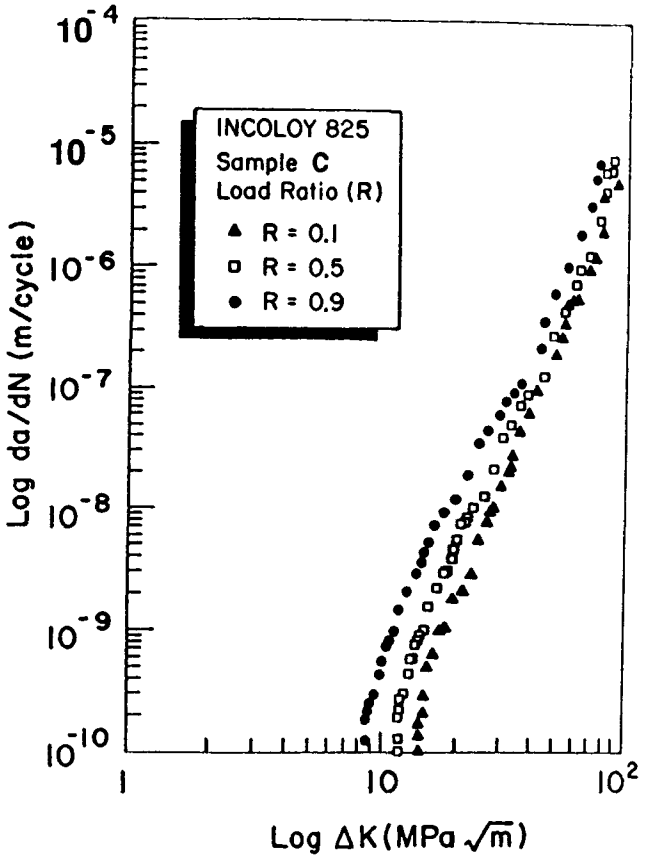

Fig. 12 Effect of load ratio on fatigue crack growth rate.

Table 6 ΔK Threshold

Sample	Condition	Load ratio, R	ΔK threshold, MPa$\sqrt{m}$
A	Non-heat treated	0.1	6.6
		0.5	4.6
		0.9	2.9
B	Heat treated under aged	0.1	12.2
		0.5	11.2
		0.9	8.4
C	Aged to peak hardness	0.1	14.4
		0.5	11.8
		0.9	8.4

with an increase in yield strength of the material. Barsom[21] also observed a linear relationship between ΔK_{th} and R. On the other hand, a nonlinear power law relationship, between threshold and load ratio, was observed by Klensil *et al.*[22] They proposed a relationship of the nature $\Delta K_{th} = \Delta K_{tho}\,(1-R)^{\gamma}$ where γ is a material environment dependent constant, *i.e.*, its value depends on the test environment.

Our test results show that none of the above relationships can sufficiently characterize the effect of load ratio on fatigue threshold in this material. The strain hardening rate (n) can significantly affect the local stress-strain field in the crack tip region. Hence, it is logical to expect that the strain-hardening exponent will have a significant effect on the stress-intensity factor (K)[23] and the cyclic hardening or softening behavior[24] of the material. The obvious conclusion is that strain-hardening rates will also have a significant influence on fatigue threshold at different load ratios. None of the relationship as previously discussed considers the effect of strain-hardening exponent on fatigue threshold. Based on these observations, a new relationship of fatigue threshold and load ratio was proposed[25] in the form of a power law relation. This proposal included the strain-hardening exponent n and the equation can be expressed as $\Delta K_{th} = (\Delta K_{tho})^{mnR}$ where m is the material environment dependent constant[25] and R is the load ratio.

The above relationship indicates that if we plot log ΔK_{th} *against* R, a straight line would be obtained. In Fig. 13, we have plotted log ΔK_{th} *versus* R for material in heat treated conditions A, B, and C. We observe indeed a straight line relationship, which validates the above hypothesis. Hence, one can conclude that the interrelation of load ratio and fatigue threshold can be characterized by the above equation.[25]

4 Conclusion

A peak hardness of 295 VHN was observed in Incoloy 825 after solution treatment at 1200 °C for ½ hr and followed by aging

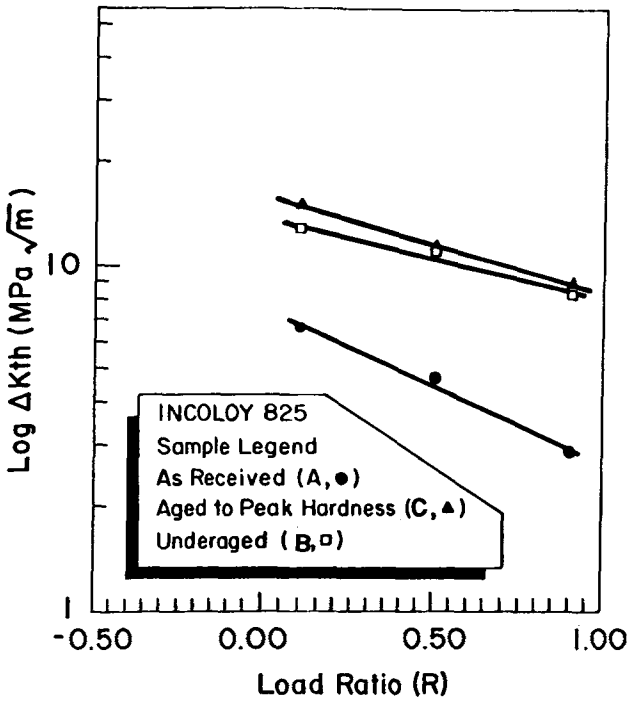

Fig. 13 Effect of load ratio on fatigue threshold.

at 600 °C for 434 hr. Fatigue threshold values were the highest and the near-threshold crack growth rate was lowest in this heat treated condition. This high strength and hardness in peak aged condition is due to very fine carbide precipitation in this material. Fatigue crack growth rate in the threshold region was found to increase with an increase in the load ratio.

A previous mathematical model describing the relationship between load ratio, fatigue threshold, and strain-hardening exponent was found applicable and characterized the influence of load ratio on fatigue threshold in Incoloy 825. The higher fatigue threshold and lower near-threshold crack growth rate in peak aged condition is apparently due to torturous crack path and secondary crackings in the material.

References

1. P.C. Paris and F. Erdogan, *J. Basic Eng. Trans. ASME*, Series D, *85*, 528-539 (1963).
2. R.O. Ritchie, *Int. Met. Rev.*, (5) and (6), 205-230 (1989).
3. R.O. Ritchie, *Met. Sci.*, *11*, 368-381 (1977).
4. C.J. Beevers, *Met. Sci.*, *11*, 362-367 (1977).
5. R.J. Cooke, P.E. Irving, G.S. Booth, and C.J. Beevers, *Eng. Fract. Mech.*, *7*, 69-77 (1975).
6. J.F. Throop and G.A. Miller, ASTM Special Technical Publication 457, ASTM, Philadelphia, 231-244 (1970).
7. S.K. Putatunda, *Trans. Ind. Inst. Met.*, *40*(1), 122-131 (1987).
8. J.P. Benson and D.V. Edmonds, *Mater. Sci. Eng.*, *38*, 179-186 (1986).
9. J.P. Benson, *Met. Sci.*, *13*, 535-539 (1979).
10. W.G. Clarke and H.E. Trout, *J. Eng. Fract. Mech.*, *2*(2), 223-238 (1970).
11. R.O. Ritchie, *J. Eng. Mater. Technol. Trans. ASME*, *99*, 195-204 (1977).
12. ASTM E-647, Annual Book of ASTM Standard, Vol 03-01, 712, ASTM, Philadelphia (1988).
13. S.K. Putatunda, A. Spis, and J. Raghavan, TMS Annual Meeting, Anaheim, CA, Feb (1990).
14. T.J. Garosshen and G.P. McCarthy, *Met. Trans.*, *16A*, 1213-1223 July (1985).
15. W. Elber, *Eng. Fract. Mech.*, *21*, 323-331 (1970).
16. R.O. Ritchie and S. Suresh, *Int. Met. Rev.*, *13*, 23-68 (1987).
17. M.J. Donachie, in *Superalloys Source Book*, M.J. Donachie, Ed., ASM, Materials Park, OH, 102-131 (1984).
18. K.S. Ravichandran, H.E. Venkatarao, E.S. Dwarakadasa, and C.G. Krishadasnair, *Met. Trans.*, *18A*, 865-876 May (1987).
19. W. Matuszyk, G. Camps, D.J. Duquette, and N.S. Stolloff, *Met. Trans.*, *21A*, 2967-2988 (1990).
20. O. Vosikovsky, *Eng. Fract. Mech.*, *11*, 595-602 (1979).
21. J.M. Barsom, *WRC Bull.*, *194*, 33-38 (1974).
22. M. Klensil and P. Lukas, *Mater. Sci. Eng.*, *9*, 231-236 (1972).
23. R.W. Hertzberg, *Deformation and Fracture Mechanics of Engineering Materials*, 3rd ed., John Wiley & Sons (1987).
24. V. Weiss and D. Lall, *Met. Trans.*, *5A*, 1946-1963 (1974).
25. S.K. Putatunda, *Trans. Ind. Inst. Met.*, *41*, 33-36 (1989).